Journal of Marine Science and Technology

Volume 26 | Issue 3 Article 13

STUDY ON STRUCTURAL ADHESIVE APPLIED TO THE BULKHEAD JOINTS SUBJECTED TO NON-CONTACT UNDERWATER EXPLOSION

Guang-Min Luo
Department of Naval Architecture and Ocean Engineering, National Kaohsiung University of Science and Technology, Kaohsiung, Taiwan, R.O.C.

Yi-Huei Lin
Department of Naval Architecture and Ocean Engineering, National Kaohsiung University of Science and Technology, Kaohsiung, Taiwan, R.O.C.

Journal of Marine Science and Technology, Vol. 26, No. 3, pp. 421-430 (2018)
DOI: 10.6119/JMST.2018.06_(3).0013

STUDY ON STRUCTURAL ADHESIVE APPLIED TO THE BULKHEAD JOINTS SUBJECTED TO NON-CONTACT UNDERWATER EXPLOSION

Guang-Min Luo and Yi-Huei Lin

Key words: bulkhead, structural adhesive, underwater explosion.

ABSTRACT

The overlapping method is commonly used in fiber-reinforced plastic (FRP) bulkhead-hull bonding. This study replaced the traditional overlap approach in using FRP components for bonding with the use of structural adhesives in the bulkhead-hull joint. A numerical simulation was conducted to investigate the structural response of the FRP-based bulkhead joint to underwater explosion shocks and examine the bonding differences between the application of structural adhesives and the traditional overlap approach. For precise estimation and shortening the numerical calculation process, solid elements were used to construct a local model using ABAQUS/Acoustic to simulate the effects of underwater explosions. In addition, two sizes of structural adhesive joint were considered for comparison with overlapping joints. The simulation results revealed that the application of structural adhesives provided an effective buffer between the hull and bulkhead by dissipating the stress from underwater explosions, reducing the maximum stress response by 67%. Moreover, although the amount of structural adhesive exhibited negligible effects on impact loading, overapplication may conversely lead to structural hardening.

I. INTRODUCTION

Noncontact underwater explosions refer to torpedo and depth charge ignition within a certain distance. Although the impact of a noncontact underwater explosion may not directly lead to vessel leakage or sinkage, the acceleration generated by the instant release of dynamic stress may produce drastic vibrations to the structure, resulting in structural and operational damage and the loss of operational capability. Therefore, in this study, structural adhesives were applied to the joint between an FRP hull and bulkhead with consideration for high toughness to withstand underwater explosions and ensure structural integrity. By comparing the difference between traditional overlap and structural adhesive overlap, this study examined the feasibility and advantages of using structural adhesive for bonding bulkheads to the hull.

FRP structures in naval vessels can be applied to attain effective ship maneuverability by reducing 35%-50% of the draft. They have greater buffering effects than metals because they eliminate vibration noises and heat conduction. Therefore, the United States has focused on developing the application of FRP composites for naval vessels since 1946. In 2001, Mouritz et al. (2001) conducted a detailed assessment on the use of composite structures in naval ships.

In the past, FRP vessels were mainly assembled using fiber joint-based bonding and structural adhesives were only used in repairing structural fractures. With recent advancements in polymer technology, structural adhesives have been widely applied in bonding the structures of vessels. In their experiment and simulation study on the properties of adhesively bonded T-joints, Zhou et al. (2008) revealed that assigning a longer length for the fillet radius can effectively eliminate the concentration of stress around the joint by distributing stress evenly on the adhesive layer and thereby elevating the strength of the T-joints. The present study adopted the Crestomer 1152-PA structural adhesive, which has a substantially high failure strain and has been widely applied in the construction of various naval ships and life boats. For instance, the Crestomer 1152-PA has been adopted as the bonding material for the upper FRP structure of the La Fayette-class frigate (Crestomer® 1152PA, 2016) and as the adhesive for bonding all structures in FF-1200 lifeboats (Crestomer structural adhesives, 2016). In Crestomer structural adhesives (2016), its strength and reliability was confirmed in a 55-m free-fall test.

Current literature and response spectra of underwater explosions were first reviewed to determine appropriate loads for numerical simulation. Recent studies on underwater explosions are presented as follows.

Experimental and theoretical validation were required in early investigations because computers and numerical software were relatively undeveloped, but the availability of innovative software simulation and numerical analysis for underwater explo-

Paper submitted 12/19/17; revised 02/14/18; accepted 05/24/18. Author for correspondence: Guang-Min Luo (e-mail: gmluo@nkust.edu.tw).
Department of Naval Architecture and Ocean Engineering, National Kaohsiung University of Science and Technology, Kaohsiung, Taiwan, R.O.C.

sions in recent years has effectively enhanced the overall accuracy of analysis and reduced the time and costs required for experiments. In a study on the response of surface vessels to underwater explosion, Shin (2004) established a 3D model of an actual vessel and used fluid-structure interaction (FSI) to simulate far-field underwater explosions. With consideration of the cavitation phenomenon in free surfaces, Gong (2006) employed the explicit finite element method (FEM) with the boundary element method to analyze floating structures' response to underwater shock and compared a two-layered panel configuration with a sandwich panel configuration. Sprague and Geers (2006) investigated the shock loading of surface vessels through experiments and simulations; in the simulation, cavitation bubbles were assumed a nonlinear acoustic medium, and accordingly, spectral elements with different orders were used to simulate fluid dynamics and construct a new simulation method. By using the Lagrangian-Eulerian computing method, Wang et al. (2014) simulated the water-air interface and shockwave-structure interaction, revealing that the boundary conditions formed by the structure's surface and free-surface flow significantly affected the acoustic properties of shock waves.

Underwater explosions involve complex factors such as high velocities, drastic compressions, deformations, and multiphase flows, rendering their numerical simulation considerably difficult. By adopting a modified smooth particle hydrodynamics method, Zhang et al. (2011) and Zhang et al. (2012) successfully simulated shock wave propagation and investigated the effects of whipping response generated by underwater explosion on vessel structures with further consideration of the wave effect. Moreover, Zhang et al. (2014) combined the FEM and the doubly asymptotic approximation (DAA) method to explore the transient response of underwater explosion bubbles on vessels; the results suggested that local structural damage generated in various directions should be considered in addition to the overall whipping response because of the bubble jetting effects of underwater explosions. Hsu et al. (2014) considered the whipping and water jetting effects induced by bubble jetting and examined underwater bubble explosion, impulse, and collapse using ABAQUS with Eulerian analysis, successfully simulating the dynamic behaviors of underwater bubbles such as migration and pressure impulse.

The DAA method is commonly adopted in underwater explosion studies. Using DAA, Gong and Lam (1999) inferred the FSI equation for local submerged vessel structures, derived the FSI response with the FEM and boundary element method, and conducted a transient analysis of a composite hull subjected to an underwater explosion, proving that boundary conditions affect the transient response of structures; in addition, the results of an analysis of the stress distribution of multidirectional underwater explosions also suggested that the bottom structure of a ship receives the maximum stress. Liang and Tai (2006) applied the DAA to investigate the transient response of naval ships to underwater explosions and considered transient dynamics, geometric nonlinearity, the properties of elastic-plastic materials, and the FSI effect, finally using the keel shock factor (KSF) to describe shock severity. This study referred to the findings of Gong and Lam (1999) to examine the processes involved in joining the bottom hull with the bulkhead.

In addition to theoretical and experimental approaches, various innovative numerical applications such as Dytran, LS-DYNA, and ABAQUS provide simulations of blast dynamics. ABAQUS is mainly applied for nonlinear underwater explosion simulations, with the choice of ABAQUS/USA and ABAQUS/Explicit; the underwater explosion simulation conducted in this study adopted ABAQUS/Explicit, which applies a coupled structural-acoustic analysis for the underwater explosion simulation, using acoustic elements to define the acoustic medium, describe shock wave propagation, and calculate the earliest surface stress induced by shock waves as well as acceleration processes, which can avoid the pressure decay of far-field explosions and attain precise modeling and simulation for the effects of added mass, pressure, wet surface area, and capillary action. Tai et al. (2006) adopted ABAQUS to simulate underwater shock response of stiffened plates with reference to experimental results from related literature. Considering the coupling elastic effect between the hull and equipment structure, Zhang et al., 2011) applied ABAQUS to model the structure of a ship and its equipment and calculate various shock responses under different explosions. Through the application of ABAQUS, Qiankun and Gangyi (2011) conducted an under-water explosion experiment on the shock response of metal hulls to investigate the difference between acceleration and velocity response when damping is considered, confirming that the experimental and simulated results were consistent. With a deterministic dynamic associative memory model, Hsu et al. (2014) integrated the induced response spectrum from an experiment on a US navy ship with ABAQUS and established an analytic method for the explosion response spectrum to evaluate the damage tolerance of submarines.

As multiple empirical formulas are required in underwater explosion simulation, a considerable number of empirical and theoretical formulas have been published. In 2005, Liang et al. (2005) verified formulas and parameters developed by Roop, Cole, Aron, Keil, Smith, and Mäkinen through numerical simulations and revealed that the theoretical formula proposed by Cole (1948) in 1948 has the highest accuracy. Accordingly, this study adopted the formula developed by Cole to retrieve related explosion parameters for further numerical simulations.

II. NUMERICAL MODEL AND MATERIALS PARAMETERS

The adopted ABAQUS/Explicit processed numerical simulations using theoretical and empirical formulas to estimate the condition of shock waves in flow fields and calculate the stress distribution in flow fields by using FSI. In addition, the ABAQUS can load the pressure field directly onto a structure to increase analysis speed.

1. Numerical Model and Joint Design

The modeling and analysis of this study referenced the design

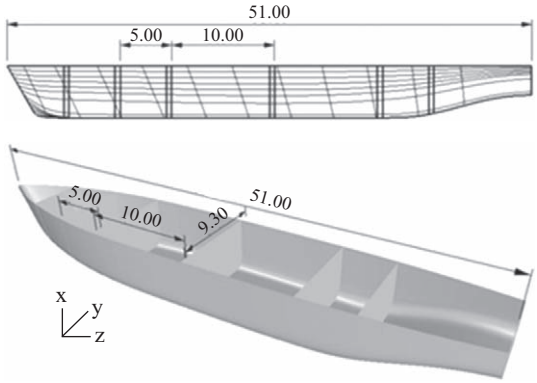

Fig. 1. Minehunter model.

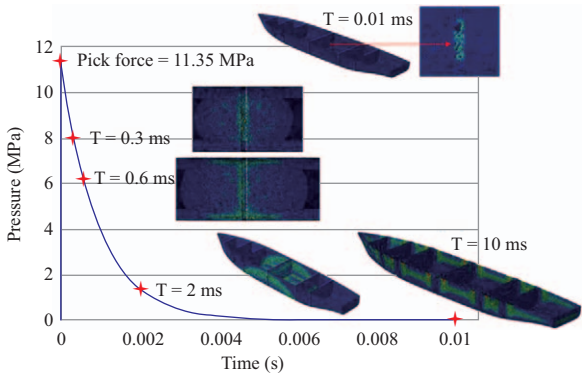

Fig. 2. Structural response varying with explosion pressure.

of the Type 332 Frankenthal-class minehunter [21], which is 51 m long and 9.2 m wide and features a 2.5-m draft load and 6 bulkheads deployed at various distances. Because the lateral and bottom thicknesses of the structure often vary under different loadings, these measurements were set as 16 cm and 20 cm, respectively. The model of minehunter considered in this study is shown in Fig. 1.

General underwater explosion analysis is often simulated using LS/Dyna or ABAQUS/USA (Underwater shock Analysis). In this study, we used ABAQUS/Explicit with acoustic tetrahedral element to simulate the structural response of hull subjected to underwater explosion. In the absence of experimental results that can be verified. We first used shell element to model the entire ship and then simulated the structural response on the hull and bulkhead. Finally, we qualitatively discussed the stress responses of hull and bulkhead subjected to explosion and compared the results with references to confirm the feasibility of the simulation method considered in this study.

Fig. 2 shows the structural responses of minehunter hull varying with time and explosion pressure. The simulation results show that when the hull is subjected to an underwater explosion, the stress response will be generated at the bottom of vessel closest to the explosion source. As the explosion pressure decreases, the stress will gradually spread out from the bottom of vessel and eventually spread to the entire hull. The maximum stress response

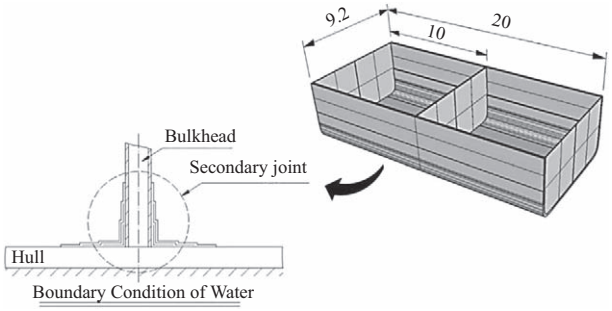

Fig. 3. Local solid element model.

occurs near the free end of the hull or the hull-bulkhead joint at this time. The explosion stress responses and phenomenon obtained by the simulation method of this study is the same as that of Liang and Tai (2006). This result proves that the simulation method considered in this study can be applied to discuss the behavior of hull-bulkhead joint subjected to underwater explosion.

Previous studies have used shell elements to establish numerical models. By contrast, this study established a local model with solid elements to investigate detailed underwater shock responses generated on the joint structure between the hull and bulkhead. Moreover, the amidships section was specifically analyzed because the structure receives greater bending effects from the tension and compression of underwater explosions. The actual local model was designed as 20 m long and 9.2 m wide and followed the explosion parameters proposed by Liang and Tai (2006); the shot point was deployed at the bottom of amidships with a KSF of 0.8; and the angle-ply laminate of the amidships section was assigned as 0°/90° for sufficient bending strength, as suggested by the analysis results of Lee (2005).

The modeling in this study adopted the solid element C3D8R, which is a reduced integration element that can be used to increase calculation efficiency by reducing integration points. The local model and the main regions of analysis are shown in Fig. 3.

Regarding the fluid boundary conditions of the water domain in the experiment, this study assumed the water surface to be a free surface and the bottom plane was assumed to show non-reflective conditions. In accordance with the suggestions of Gong and Lam (1999), the local model of this study applied simply supported boundary conditions and horizontal and longitudinal movement was limited in order to enable the structural responses to be consistent with that of the overall model. In addition, to eliminate the boundary effects of the water domain, the width of the water domain is suggested to be 6 times greater than that of the ship. Therefore, the water domain was designated as being 56 m wide and 28 m deep (Fig. 4) and having 1025 kg/m^3 fluid density and 1500 m/s sound velocity. The AC3D4 acoustic tetrahedral element was adopted to simulate the fluid behavior in the domain.

Three layers of fiber-reinforced composites were adopted for the traditional overlapping joint. The bottom layer was 50 mm long. The length of the second layer was 75 mm so as to cover the first layer. Similarly, the third layer was extended to

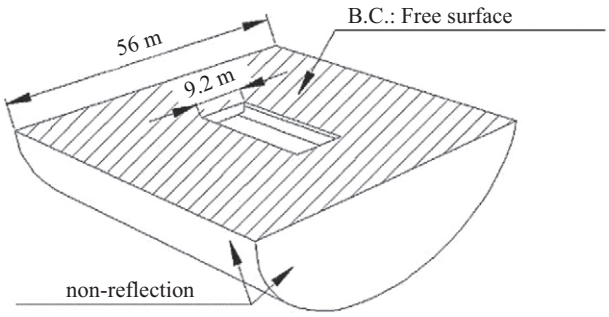

Fig. 4. Water domain.

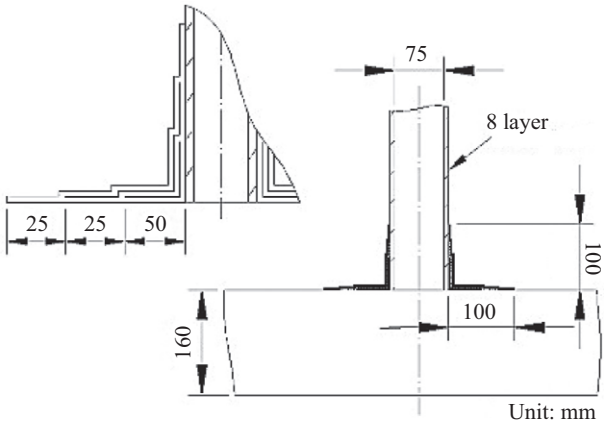

Fig. 5. Overlapping size of OL series.

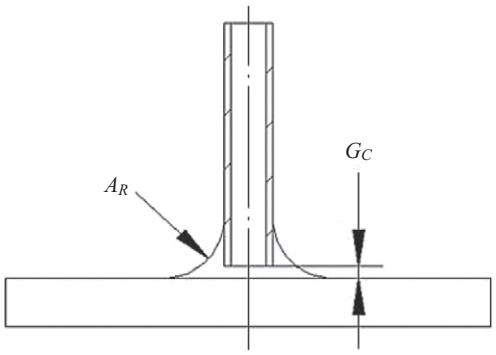

Fig. 6. Bonding shape-suggested by Crystic Crestomer.

100 mm in order to cover the second layer. High-tolerance DERAKANE 8084 epoxy vinyl ester resin was used. The overlapping joint structures proposed in this study were named the OL series, and the overlapping method and joint sizes are indicated in Fig. 5. Additionally, the design of the other adhesively bonded joint is shown in Fig. 6.

The bonding method and specifications of the 1152-PA structural adhesive was devised with reference to official suggestions from Scott Bader Co. Ltd (2008). According to the official application guide, the space between the bulkhead and hull (G_c) should exceed 10 mm and the joint should feature a fillet with a

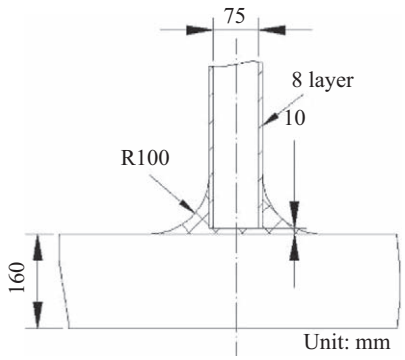

(a) AR-100

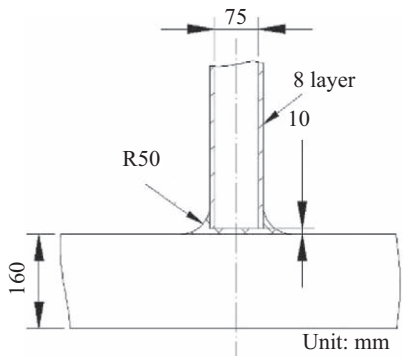

(b) AR-50

Fig. 7. Designs and specifications of AR-100/AR-50.

radius of no less than 25 mm (A_R) for bonding. Therefore, the fillet radiuses of the two joints were assumed to be 50 mm and 100 mm and the joints were named the AR-50 and AR-100 series, respectively. The designs and specifications of the AR-50 and AR-100 series are displayed in Fig. 7.

2. Mesh Sizes of Local Solid Element Model and Water Domain

Underwater explosion analysis is a highly nonlinear problem. Therefore, the mesh size of FEA model will affect the accuracy and convergence of underwater explosion analysis. In this study, we tried different mesh sizes to create FEA model and simulated its structural responses. The test results found that appropriate meshes can improved analysis convergence, but not the smaller the better. Following are descriptions of mesh sizes considered in this study.

AC3D4 acoustic tetrahedral element was used to simulate the transmission of shock wave in water domain. The mesh size closed to the non-reflective boundary was 3 m, but the mesh size closed to the hull was 0.3 m. The FE mesh sizes of water domain and FRP hull considered in this study was shown in Fig. 8.

Furthermore, we used solid element C3D8R to simulate the responses of FRP hull, bulkhead and structural adhesive when they were subjected to underwater explosion. In addition to the corners of structural adhesive, the rest of the structures were simulated using hexahedron elements. The mesh size of hull was

Table 1. Material parameters of LT800/M225 (Khalili and Ghaznavi, 2011).

Ex (MPa)	X[a] (MPa)	Ey (MPa)	Ez (MPa)	Gxy (MPa)	Gyz (MPa)	Gzx (MPa)	v	ρ (kg/m^2)
18096.3	398	18096.3	3550	3106.3	1500	1500	0.22	1689.48

[a] X is failure strength of material.

Table 2. Material parameters of Divinycell H100 PVC (Khalili and Ghaznavi, 2011).

Ex (MPa)	X (MPa)	Ey (MPa)	Y (MPa)	Gxy (MPa)	S (MPa)	v	ρ (kg/m^2)
105	2.4	105	2.4	40	1.4	0.3	100

Table 3. Material parameters of Crestomer 1152-PA (Khalili and Ghaznavi, 2011).

Ex (MPa)	X (MPa)	Ey (MPa)	Y (MPa)	Gxy (MPa)	S (MPa)	v	ρ^2 (kg/m^2)
500	15	500	15	170	8.7	0.47	1050

[a] Data source from Crestomer structural adhesives (2016).

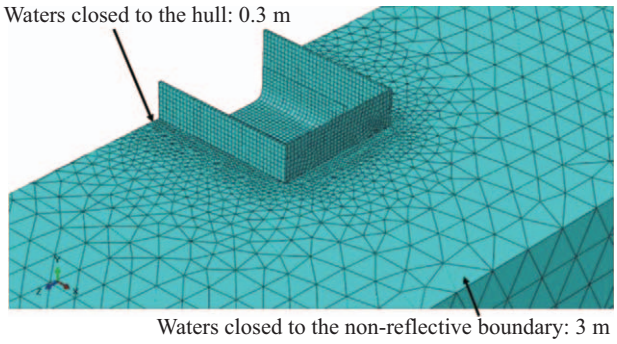

Fig. 8. FE mesh sizes of water domain and hull.

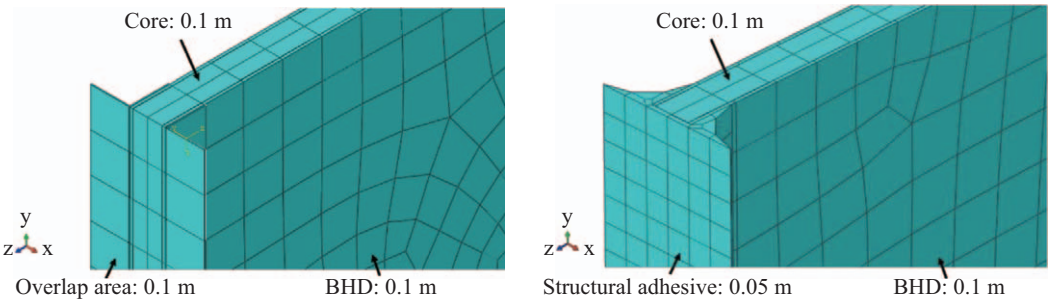

(a) OL series model (b) AR series model

Fig. 9. FE mesh sizes of local solid model.

the same as water domain, which was 0.3 m. The mesh sizes of bulkhead, core and overlapping joints were 0.1m. In this study, we mainly discussed the behavior of structural adhesive delivering the explosion loadings. Therefore, the mesh sizes of structural adhesive considered in this study was 0.05 m. The structural meshes of local solid model were shown in Fig. 9.

3. Material Parameters

This study used LT800/M225 fiber and DERAKANE 8084 epoxy vinyl ester resin, and the hull was assumed to have been manufactured using vacuum-assisted resin transfer molding (fiber content: $W_f = 61\%$). The material parameters of the laminated LT800/M225 fiber can be inferred using the classical laminate theory (Table 1). In addition, the bulkhead featured a sandwich panel configuration, with Divinycell H-100 PVC foam as the core material; the material parameters of the proposed core material and structural adhesive were devised according to Zhou (2008) and Khalili and Ghaznavi (2011) (Tables 2 and 3).

Table 4. Cohesive properties of Adhesive Crestomer 1152-PA Crestomer structural adhesives (2016).

K_{nn} (MPa)	$K_{ss} = K_{tt}$ (MPa)	σ_{nn} (MPa)	$\sigma_{ss} = \sigma_{tt}$ (MPa)	G_{Ic} (J/m^2)	G_{IIc} (J/m^2)
500	170	15	8.7	150	300

Table 5. Cohesive properties of vinyl ester DERAKANE_8084.

K_{nn} (MPa)	$K_{ss} = K_{tt}$ (MPa)	σ_{nn} (MPa)	$\sigma_{ss} = \sigma_{tt}$ (MPa)	G_{Ic} (J/m^2)	G_{IIc} (J/m^2)
3297	1040	72.8	39.5	307	490

[a.] Data source from Stevanovic (2003); [b.] Data source from Dale et al. (2012); [c.] Data source from Crestomer structural adhesives (2016).

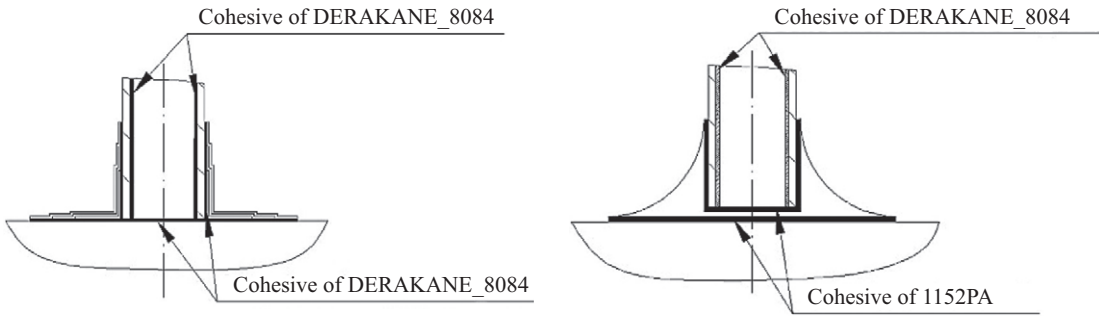

(a) Interface of overlapping (b) Interface of structural adhesive

Fig. 10. Cohesive contact surface.

ABAQUS can use cohesive element and cohesive surface to simulate the interface destruction behavior of the adhesion. In this study, we chose cohesive surface to simulate the glued interface and used maximum nominal stress criterion to determine damage initiation of adhesion interface. In addition, ABAQUS provides four damage models to define the damage evolution. We chose fracture energy method and Benzeggagh-Kenane evolution law defined by ABAQUS to determine the damage parameters and simulate the process of joint failure.

This study adopted cohesive contact surfaces to simulate the damage at the overlapping and adhesively bonded interface; the numerical model is indicated as Fig. 10. Certain related damage parameters should be provided when cohesive surface is used to model damage behavior in ABAQUS, including separation stiffness, damage initiation, and fracture energy. When ABAQUS detects corresponding damages on the adhesively bonded structures during numerical simulation, material rigidities are automatically modified according to the criterion of damage evolution.

In addition, as per the suggestions of Shawish et al. (2013), the present study assumed the separation stiffness of the cohesive surface to be the tensile and shear modulus when the interface thickness approximated zero. As the present study's focus is on the effects of different hull-bulkhead bonding methods on their joint components' resistance to underwater shock loading, related damage parameters developed in previous studies were directly adopted in the present study. Specifically, the damage parameters for the Crestomer 1152-PA structural adhesive referenced Zhou (2008), and the parameters for the DERAKANE 8084 epoxy vinyl ester resin partially adopted the experimental and simulated results of Stevanovic (2003), Dale et al. (2012), and Compston et al. (2001). The damage parameters for the materials are listed in Tables 4 and 5.

4. Underwater Explosion Parameters

In the ABAQUS/Acoustic underwater explosion simulation, the bulk modulus was selected as the acoustic fluid medium; as suggested by ABAQUS, the bulk modulus of seawater was set as 2250 MPa, and the material property was designated as homogenous.

The KSF is a crucial reference for the design of blast-resistant surface vessels, and can also be used to determine the size of the explosive charge and the distance of the explosion. Different hull structures and ship equipment may result in differing KSF. The KSF equation is shown as (1); specifically, W denotes the weight of the explosive charge; R represents the distance between the point of measurement and the shot point; and lastly, α represents the included angle of the shockwave direction and gravity. The explosion parameters were determined according to Liang and Tai (2006); the KSF was first assigned as 0.8 and the shot point was set as 30 m directly below the bottom of the ship. Because the angle of explosion was 0°, the weight of the explosive charge was inferred to be 576 kg. Fig. 11 displays the location of the shot point.

$$KSF = \frac{\sqrt{W}}{R} \times \frac{1+\cos\alpha}{2} \tag{1}$$

Among various theoretical equations on explosions proposed

Table 6. TNT explosion constants Liang and Tai (2006).

K_1	A_1	K_2	A_2
52.12	1.18	0.00895	-0.185

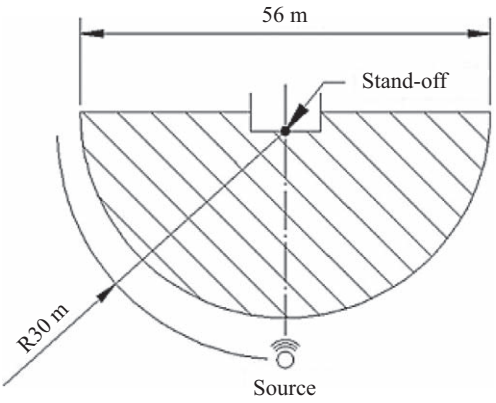

Fig. 11. Location of explosion source.

in previous studies, the most widely adopted is the underwater explosion theory developed by Cole (1948) in 1948.

$$P(T) = P_{\max} e^{-\frac{t}{\alpha}}, t \geq \alpha \quad (2)$$

$$P_{\max} = K_2 W^{\frac{1}{3}} \left(\frac{W^{\frac{1}{3}}}{R} \right)^{A_2} \quad (3)$$

$$\theta = K_2 W^{\frac{1}{3}} \left(\frac{W^{\frac{1}{3}}}{R} \right)^{A_2} \quad (4)$$

In Table 6, P_m indicates the peak shockwave pressure; θ denotes the decay constant; W refers to the weight of explosive charge, R is the distance between the measurement point and the shot point; and K_1, A_1, K_2, A_2 represent the constants for explosive charge. By substituting known parameter values into (2)-(4), a pressure-time curve for a TNT explosion shockwave is derived (Fig. 12). The figure reveals that the pressure peak first achieves a maximum value at 0.01 ms and the pressure (P) begins to show exponential decay, approximating zero at 4 ms and beyond.

III. RESULTS AND DISCUSSION

In the simulation of the underwater shock response of the hull-bulkhead joint, the study identified that the transmission of the explosion force was consistent with the conclusions of Gong and Lam (1999) and Liang and Tai (2006) The explosion force gradually dispersed from the vertical intersection between

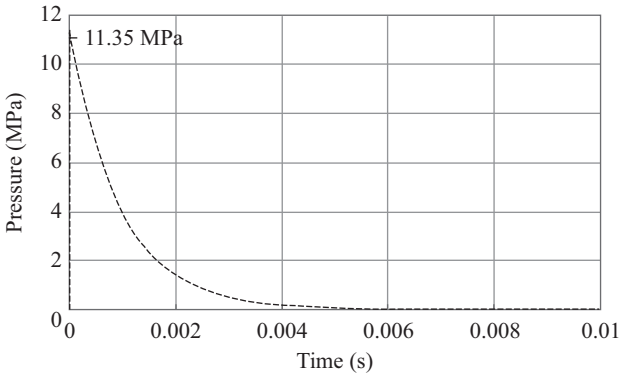

Fig. 12. Explosion progress of shock wave.

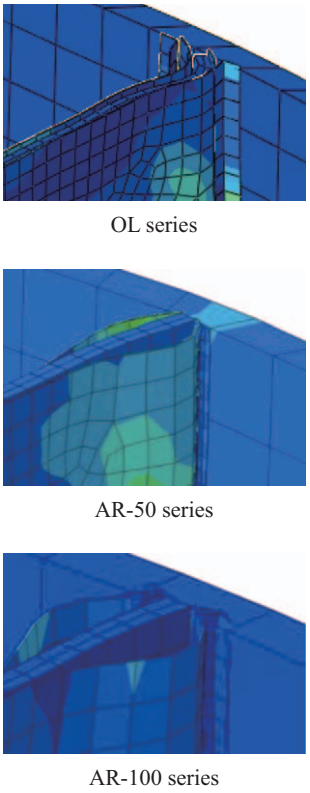

Fig. 13. Failure modes of different joints (8 ms).

the hull and the shot point to each structure of the vessel, and the various maximum stress on the joint were observed on the laminate plate of the bulkhead. The order of stress was OL > AR-50 > AR-100. Although the stress values were the greatest in the OL series, the values remained lower than the maximum fracture stress (398 MPa) of the laminate plate.

1. Failure Modes of Hull-Bulkhead Joint

We discussed the joint failure modes of different hull-bulkhead joint model subjected to underwater explosion in this study. According to numerical simulation results, the local hull model considered in this study will have the maximum structural re-

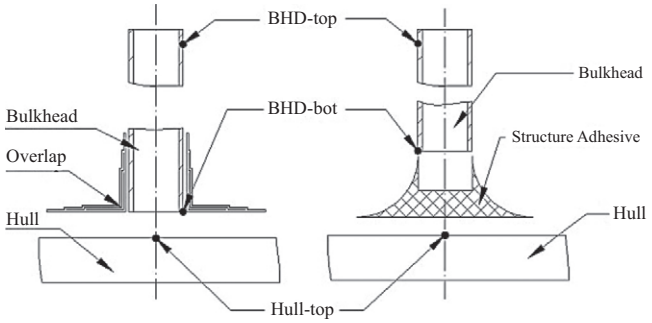

Fig. 14. Nomenclature of discussion points.

sponse when the duration time is about 8 ms. Therefore, we investigate the failure modes of the free end of bulkhead at 8 ms first.

Fig. 13 shows the failure modes of different joints when time is 8 ms. The simulation results show that OL series has a significant hard point at the hull-bulkhead joint, so it will easily break at the joint when subjected to underwater explosion. In addition, we assume that structural adhesives can effectively transfer explosive energy and increase hull-bulkhead joint strength. The simulation result shows that the destruction of AR-50 series occurred at the sandwich panel of bulkhead, which was in line with the initial hypothesis of this study. However, the AR-100 series has been damaged in the bulkhead and hull-bulkhead joint. This result shows that excessive structural adhesive will also produce hard point at the hull-bulkhead joints, which will cause stress transfer difficulties. Therefore, a proper glue range is necessary.

2. Discussion of Joint Responses

Considering how the bottom hull structure receives the most severe explosion shocks Gong and Lam (1999), the joint bonding the bottom structure and bulkhead were the focuses of further examination. Fig. 14 indicates the three regions analyzed, including the inner region of the bottom hull (Hull-bot), the root-end of the joint bonding the bulkhead and bottom hull (BHD-bot), and the top region of the bulkhead near deck level (BHD-top).

According to the simulation results for Hull-bot (Fig. 15), differences in bulkhead joints did not affect the occurrence time of the maximum stress, but noticeable differences was observed in the stress response of the bottom hull. For instance, the stress response in the traditional overlap OL series amounted to 65.39 MPa, which was markedly (approximately 1.7 times) greater than those of the adhesively bonded AR-100 and AR-50 series. This result indicates that the use of structural adhesive increased the elasticity of the joint, and absorbed the initial explosion shockwaves to effectively reduce the shock loading on the bottom hull. In addition, the stress responses of the inner plate of bottom hull in the AR-100 and AR-50 series were nearly identical, and the peak stress values occurred at approximately the same time. Therefore, applying additional structural adhesive was revealed to have limited effects in deferring shock loading. The peak stress values and their corresponding time are shown as Table 7.

Table 7. The peak stress and corresponding time for measure point-"Hull-bot".

	OL	AR100	AR50
Time (ms)	5.95	5.95	5.98
Max Stress (MPa)	65.39	38.43	38.89

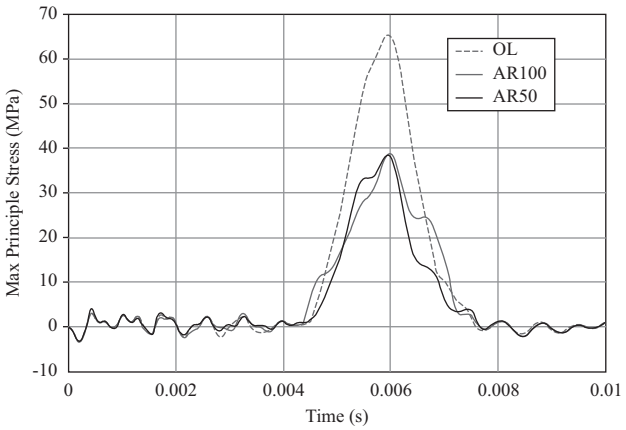

Fig. 15. Stress responses varying with time-"Hull-bot".

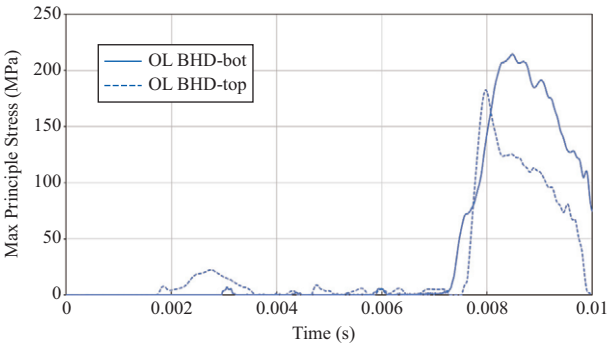

Fig. 16. Stress responses varying with time-OL-series bulkhead.

Fig. 16 shows the stress responses changes in the two observation points on the OL-series bulkheads across time. The maximum stress response of the bulkhead-bottom hull joint occurred at 8.48 ms (214 MPa) and that of the top bulkhead near the deck occurred at 7.98 ms (182 MPa). The difference between the maximum stress responses generated in the two regions was negligible, suggesting that the shock load received in the bottom hull plate was eventually transmitted to the overall bulkhead structure.

Figs. 17 and 18 display the stress response changes of the AR-100 and AR-50 series bulkhead from two observation points. The analysis results indicate that structural adhesive can effectively buffer shock load. Thus, the maximum stress responses observed in the AR series were only half of those in the OL series. In addition, in the BHD-top measurements, the maximum stress response of the AR-100 series was slightly lower than that of the AR-50 series (111.5 MPa vs. 126.34 MPa), indicating that greater amounts of structural adhesives can defer the transmission of shock loading on bulkheads. However, the analysis re-

Table 8. The peak stress and corresponding time for measure point at BHD.

series		OL	AR-100	AR-50
BHD-bot	Time (ms)	8.48	8.47	8.94
	Max Stress (MPa)	214.45	94.89	69.48
BHD-top	Time (ms)	7.98	8.06	8.92
	Max Stress (MPa)	182.27	111.5	126.34

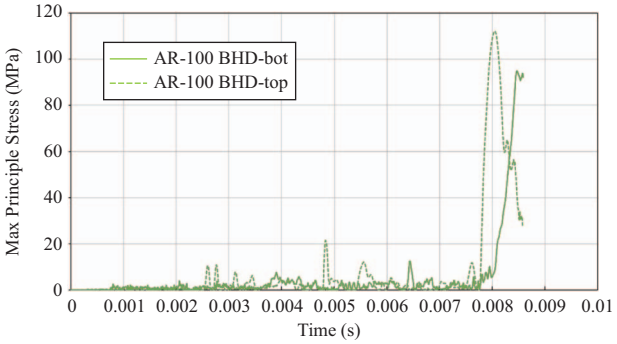

Fig. 17. Stress responses varying with time-AR-100 bulkhead.

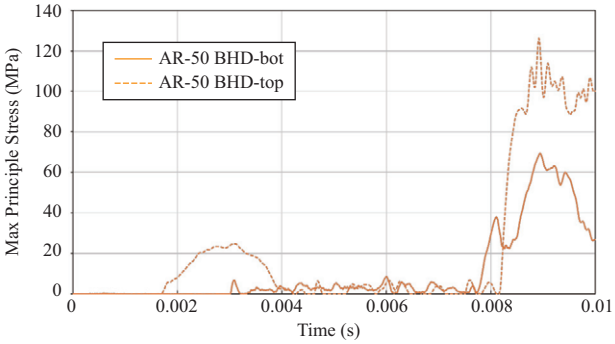

Fig. 18. Stress responses varying with time-AR-50 bulkhead.

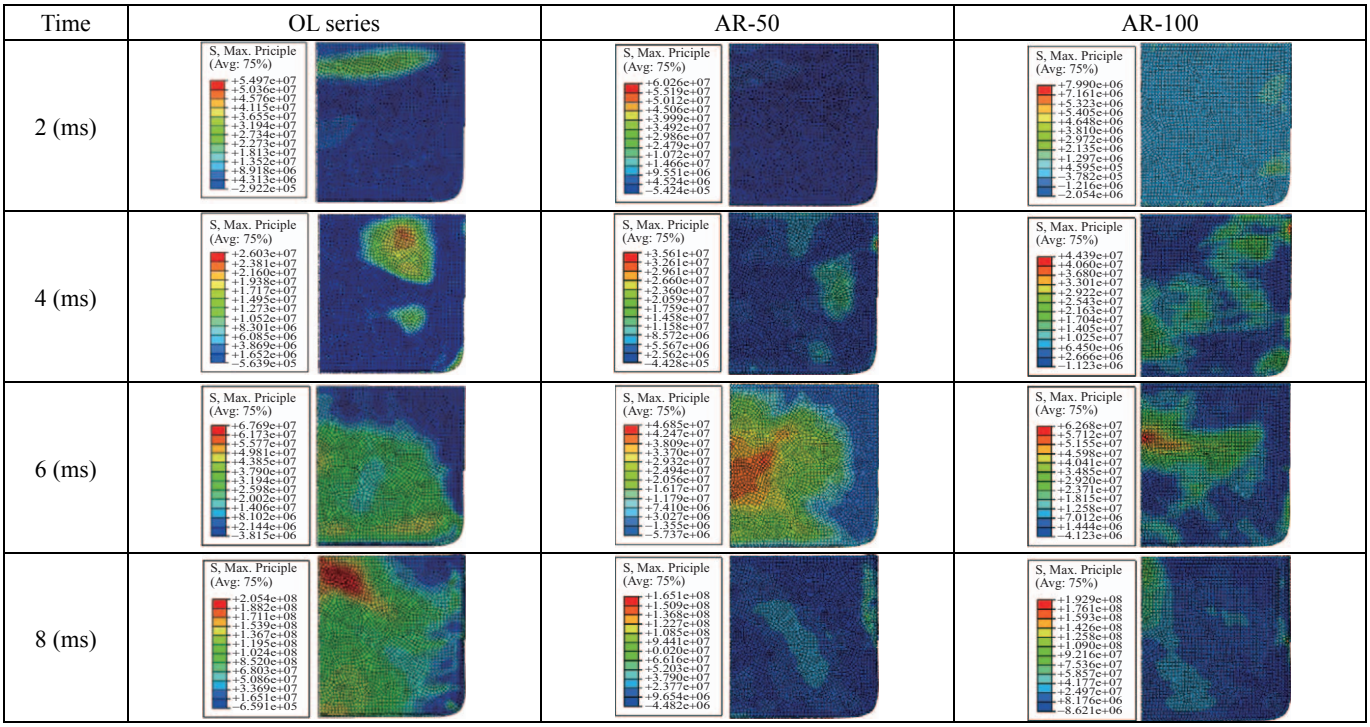

Fig. 19. Stress responses of BHD.

sults for BHD-bot revealed that the stress value in AR-100 was markedly higher than that in the AR-50 series (94.89 MPa vs. 69.48 MPa). This suggests that excessive use of structural adhesive may lead to structural hardening and a limited degree of freedom, leading to higher stress responses. Thus, greater amounts of structural adhesive may cause unforeseen damage to the joint structures. The maximum peak stress and occurrence time observed on the bulkhead are tabulated in Table 8.

Although the shock resistance capacity in the form of blocking the transmission of shock loading identified in the AR-50 series was slightly inferior to that of the AR-100 series, the greater amounts of structural adhesive in the AR-100 series can limit the structure's degree of freedom, and may thus affect the dissipation of shock energy and lead to a higher incidence of damage. Therefore, the AR-50 design was relatively safer for enhancing hull-bulkhead bonding.

Finally, we discuss the stress transmission and distribution on the bulkhead after the underwater explosion load transmitted through different joints. The structural response changes in the joint series across time are shown in Fig. 19. In Fig. 19, we can find the stress responses of AR-50 series are lower than OL and AR-100 series when the explosion duration times are 6 ms and 8 ms. This result shows that the OL series had faster stress transmissions, whereas the transmissions in the AR-50 series were slower than in the AR-100 series, revealing that applying additional amounts of structural adhesive may not necessarily enhance performance.

This stress transfer response can also explain why the maximum stress response of the BHD-top observation point occurred earlier than BHD-bot's in Figs. 16-18. Harder joints are more direct in stress transmission, and the BHD-top observation point is close to the free end of bulkhead. It is easy to cause large stress response due to obvious deformation of bulkhead. As the result, the maximum stress response of BHD-top may occur earlier than BHD-bot. Fig. 16 (AR-100 series) is a very obvious example.

IV. CONCLUSIONS

This study successfully used a local solid finite element model to simulate the shock responses of hull-bulkhead joints subject to noncontact underwater explosions. The results revealed that the stress responses on the inner hull plate in the AR series were 41% lower than the OL series. In addition, the application of structural adhesive can effectively reduce the stress response on the joint and eliminate up to 67% of the stress on the bulkhead. These results confirmed that structural adhesives may be used to enhance elasticity between the hull and bulkhead and effectively alleviate the stress response on the hull structures from shock loading.

Regarding the area range for adhesive bonding, the official guide for Crestomer recommends using a fillet radius greater than 25 mm. By applying 50-mm and 100-mm fillet radii, this study verified that greater applications of structural adhesive limit the effects of shock resistance, and revealed that excess use of the adhesive may lead to a limited degree of freedom, stress concentration, and joint damage. Therefore, this study suggests that the range of the AR-50 series is sufficient for bonding.

ACKNOWLEDGEMENTS

The authors would like to thank the Ministry of Science and Technology of the Republic of China for financially supporting this research.

REFERENCES

Crestomer structural adhesives issue (2016). Available: http://issuu.com/18178/docs/crestomer.

Cole, R. H., Underwater Explosions, Princeton University Press, Princeton, New Jersey, USA (1948).

Compston, P., P. B. Jar, P. J. Burchill and K. Takahashi (2001). The effect of matrix toughness and loading rate on the mode-II interlaminar fracture toughness of glass-fibre/vinyl-ester composites. Composites Science and Technology 61(2), 321-333.

Dale, M., B. A. Acha and L. A. Carlsson (2012). Low velocity impact and compression after impact characterization of woven carbon/vinylester at dry and water saturated conditions. Composite Structures 94(5), 1582-1589.

Gong, S. W. and K. Y. Lam (1999). Transient response of floating composite ship section subjected to underwater shock. Composite Structures 46(1), 65-71.

Gong, S. W. and K. Y. Lam (2006). On attenuation of floating structure response to underwater shock. International Journal of Impact Engineering 32(11), 1857-1877.

Hsu, C. Y., C. C. Liang, A. T. Nguyen and T. L. Teng (2014). A numerical study on the underwater explosion bubble pulsation and the collapse process. Ocean Engineering 81, 29-38.

Hsu, C. Y., C. C. Liang, T. L. Teng and Q. D. Xie (2014). Shock resistant analysis of radar mount and diesel-electric engine mount of submarine. Taiwan society of naval architects and marine engineers 33(3), 145-154.

Khalili, S. M. R. and A. Ghaznavi (2011). Numerical analysis of adhesively bonded t-joints with structural sandwiches and study of design parameters. International Journal of Adhesion and Adhesives 31(5), 347-356.

Lee, Y. J. (2005). Structure mechanics for FRP ships. Taiwan society of naval architects and marine engineers 24(4), 185-202.

Liang, C. C. and Y. S. Tai (2006). Shock responses of a surface ship subjected to noncontact underwater explosions. Ocean Engineering 33(5-6), 748-772.

Liang, C. C., Y. S. Tai and T. H. Liu (2005). A study of the effects of underwater explosions. Taiwan society of naval architects and marine engineers 24(1), 39-47.

Mouritz, A. P., E. Gellert, P. Burchill and K. Challis (2001). Review of advanced composite structures for naval ships and submarines. Composite Structures 53(1), 21-42.

Qiankun, J. and D. Gangyi (2011). A finite element analysis of ship sections subjected to underwater explosion. International Journal of Impact Engineering 38(7), 558-566.

Scott Bader Company Ltd (2016). Crestomer® 1152PA. Available: http://www.scottbader.com/adhesives/selector/315/crestomer-1152pa.

Sandia national labs Albuquerque NM, Shock and Vibration Symposium Held in Albuquerque, New Mexico, vol. 2 (1988).

Shawish, S. E., L. Cizelj and I. Simonovski (2013). Modeling grain boundaries in polycrystals using cohesive elements: Qualitative and quantitative analysis. Nuclear Engineering and Design, 261, 371-381.

Shin, Y. S. (2004). Ship shock modeling and simulation for far-field underwater explosion. Computers & Structures 82(23-26), 2211–2219.

Sprague, M. A. and T. L. Geers (2006). A spectral-element/finite-element analysis of a ship-like structure subjected to an underwater explosion. Computer Methods in Applied Mechanics and Engineering 195(17-18), 2149-2167.

Stevanovic, D. (2003). Mode I and mode II delamination properties of glass/vinyl-ester composite toughened by particulate modified interlayers. Composites Science and Technology 63(13), 1949-1964.

Tai, Y. S., S. W. Mao and C. Y. Hsu (2006). The dynamic response analysis stiffened plates to underwater explosion. Taiwan society of naval architects and marine engineers 25(1), 35-46.

Wang, G., S. Zhang, M. Yu, H. Li and Y. Kong (2014). Investigation of the shock wave propagation characteristics and cavitation effects of underwater explosion near boundaries. Applied Ocean Research 46, 40-53.

Zhang, A. M., W. X. Zhou, S. P. Wang and L. H. Feng (2011). Dynamic response of the non-contact underwater explosions on naval equipment. Marine Structures 24(4), 396-411.

Zhang, A., L. Zeng, X. Cheng, S. Wang and Y. Chen (2011). The evaluation method of total damage to ship in underwater explosion. Applied Ocean Research 33(4), 240-251.

Zhang, A., W. S. Yang and X. L. Yao (2012). Numerical simulation of underwater contact explosion. Applied Ocean Research 34, 10-20.

Zhang, N., Z. Zong and W. Zhang (2014). Dynamic response of a surface ship structure subjected to an underwater explosion bubble. Marine Structures 35, 26-44.

Zhou, D. W., L. A. Louca and M. Saunders (2008). Numerical simulation of sandwich t-joints under dynamic loading. Composites Part B: Engineering 39(6), 973-985.